Preprints of the 21st IFAC World Congress (Virtual)
Berlin, Germany, July 12-17, 2020

Lithium Battery Model Development and Application in Simulation of the Energy Consumption of Electric Bus Running ⋆

Feng Xie * Olaf Czogalla ** Sebastian Naumann ***

* *Institute of Automation and Communication, Magdeburg, Germany (e-mail: Feng.Xie@ifak.eu).*
** *Institute of Automation and Communication, Magdeburg, Germany (e-mail: Olaf.Czogalla@ifak.eu).*
*** *Institute of Automation and Communication, Magdeburg, Germany, (e-mail: Sebastian.Naumann@ifak.eu).*

Abstract: Battery electric buses take an increasingly larger market share and attract much attention from bus fleet operators to undercut urban emissions limits. But meanwhile it also becomes a challenge to operators to determine the required battery capacity to be sufficient for the specific transport operations. The deployment planning includes to select appropriate bus model specifications, battery characteristics, charging parameters, timetable schedules and further dependencies under the aspect of ownership costs. Regarding battery characteristics however, most electrochemical battery models focus more on the internal structure, which have a worse compatibility on a system level. This paper aims to build up a lithium-battery model based on the third-Thevenin equivalent circuit, considering both complexity and accuracy. Firstly, this battery model is implemented with lookup tables to represent the values of each circuit component, which results in a mean error of 1.98 mV or 0.06%, compared with the original measurement data. Then a general control model of electric vehicles is introduced to cooperate with this battery model in a system, combined by the current flowing between these two models. Finally a simulation is proceeded, employing the real data from *Solaris® Urbino* 12 *Electric Bus*, which provides a reliable SOC estimation for the full day operation.

Keywords: Telecommunication-based automation systems, Smart energy, Electric buses, Battery models

1. INTRODUCTION

According to the Paris Agreement approved by more than 190 countries, the global warming has to be limited with a temperature increase less than 2 °C, defined in UNFCCC (2015). One of the main effective methods is to cut down the emission of the greenhouse gas (GHG) like CO_2, in which the transport sector plays a great role (see Grijalva and López Martínez (2019), Aber (2016), Asaithambi et al. (2017)). Many organizations and cities have developed their own policies and goals on the climate control, e.g. European Commission (2011) set the targets to reduce GHG 20% in 2020, 40% in 2030 and 80% in 2050. Nowadays, the transformation from diesel buses to electric buses is viewed as one of the key policies to achieve such climate goals (see Göhlich et al. (2014), Krawiec et al. (2016) and Adheesh et al. (2016)). Therefore, many countries established different programs to encourage the development of electric buses, such as the *Electric Mobility* in Germany (see BMU (2018)), the *Ten Cities and Thousand Vehicles* and *Green Bus Fund* respectively in China and the UK, reported by Li (2016). Due to the energy regeneration and the advantage of zero emission during driving, battery-electric buses (BEBs) are widely employed.

Simultaneously, varieties of energy plans with different types of batteries are provided by the suppliers. Du et al. (2019) evaluated the current energy storage systems (ESSs) for BEBs in Chinese market, which is shared mainly by lithium iron phosphate (LFP) batteries, lithium nickel cobalt aluminum oxide (NCA) batteries, lithium manganese oxide (LMO) batteries, nickel metal hydride (NiMH) batteries, lithium titanate (LTO) batteries, super capacitors and further emerging battery technologies. Therefore it is difficult for bus manufacturers and fleet operators to decide which types and capacities of batteries to be implemented on BEBs. It is necessary for them to forecast the energy consumption by a running BEB on a specific bus route, in order to choose appropriate locations for charging stations and schedules for fast and slow charging. Therefore, a battery model is required to simulate these behaviours on a system level. Gao et al. (2002) presented a dynamic lithium battery model for system simulation. Huria et al. (2012) built up a high fidelity model of high power lithium battery cells. Tang

⋆ Research in this paper is based on the project "*PLATON-Planning Process and Tool for Step-by-Step Conversion of the Conventional or Mixed Bus Fleet to a 100% Electric Bus Fleet*", which is funded by German Federal Ministry of Transport & Digital Infrastructure (BMVI) under grant number 03EMEN17 and co-funded by the European Commission under the framework of "Electric Mobility Europe"

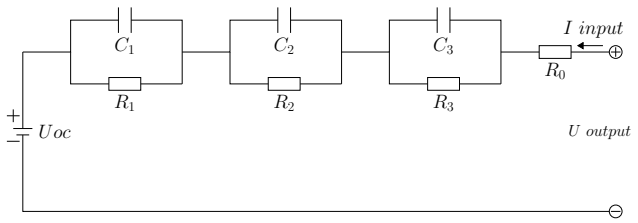

Fig. 1. Third-order Thevenin circuit.

et al. (2019) put forward a new migrated li-battery model to compensate uncertainties of temperature and ageing. In general, system-level li-battery models are developed based on the Thevenin equivalent circuit model. The higher the order is, the higher the accuracy to be obtained, but the computation will become really heavy-weighted (see Jackey et al. (2013)). As a critical part, parameter estimation could not only be time consuming but also have a high demand on device and existing tool boxes of a specific software. As a result, this paper presents a simplified third-order lithium-battery model considering both the complexity and accuracy. It uses a third order exponential equation to fit experimental data directly rather than the curve-fitting tool box to calculate step by step.

The organization of this paper is as follows: The most basic formulation for the equivalent circuit model is introduced in Section 2. All parameters of circuit elements are estimated in Section 3. Error analysis is proceeded in Section 4. In Section 5, this battery model is further connected with a general electric vehicle model for a real BEB running simulation. Finally the paper is concluded in Section 6.

2. EQUIVALENT CIRCUIT MODEL FORMULATION

Compared with electrochemical models (see Smith et al. (2007) and Klein et al. (2013)), equivalent circuit models have a better description on the behaviour of power supply to the outside modules. In order to balance both the accuracy and complexity, the Third-order Thevenin Model is adopted in this work.

Different from the general equivalent circuits for other types of batteries (e.g. the lead-acid battery model developed by Ceraolo (2000)), the self-discharge effect (i.e. parasitic branch) can be neglected for lithium-batteries (see Jackey et al. (2013)). As shown in Fig. 1, there are three parallel branches of capacitances and resistances connected in series to describe the delay effect of the output voltage U_{output}. As known, internal resistance R_0 exists normally in almost all types of batteries.

As described by Yan et al. (2018), U_{output} can be represented by (1), where U_{oc} is the open-circuit voltage of the battery, U_1~U_3 are the voltages for parallel branches of C_1~C_3, and I is the input current I_{input}.

$$U_{output} = U_{oc} + IR_0 + U_1 + U_2 + U_3. \quad (1)$$

3. PARAMETER ESTIMATION

Normally, the values of components in this equivalent circuit are irregular, which could be better represented by lookup tables based on measurement data at different states of charge (SOC).

Fig. 2. Instrumental set-up for voltage measurement.

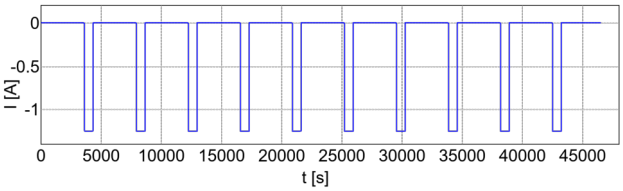

Fig. 3. Discharging current pulses.

3.1 Experimental Data Collection

Battery Selection In this experiment, one of the most widely used and environmental friendly batteries, LFP battery is selected with parameters shown in Table 1.

Table 1. LFP battery cell

Manufacturer	A123 Systems®
Model	ANR26650M1-B
Rated Capacity	2500 mAh
Nominal Voltage	3.3 V

Experimental Environment The terminal voltage of this LFP battery cell is measured at room temperature with the instrument c't-Lab®, which can collect data at a high frequency then transfer the values to the computer via a COM port, as shown in Fig. 2.

Software LabVIEW® is used to generate current pulses to control the charging or discharging process. To simplify the measurement, the battery cell is discharged from a fully-charged state to a fully-discharged state with 10% of the charged capacity. In other words, the SOC decreases 0.1C at each discharging pulse from 100% to 0%. Therefore, the discharging current is set to be 0.5C, the period for discharging is 12 min, the recovery time is 1 h, which is long enough for the battery to cool down and reach a stable state (see Fig. 3).

When the charging or discharging behaviour ends (i.e. $I = 0$), U_{output} needs a period of time to approach a stable status, which is described by the time constant $\tau = RC$. Therefore, (1) can be transformed into (2) at this moment. Voltages $U_1(0)$~$U_3(0)$ represent respectively the initial voltage of each RC branch. In this condition, $U_{output}(t)$ can be viewed as the zero-input state response, e.g. period b~c in Fig. 4.

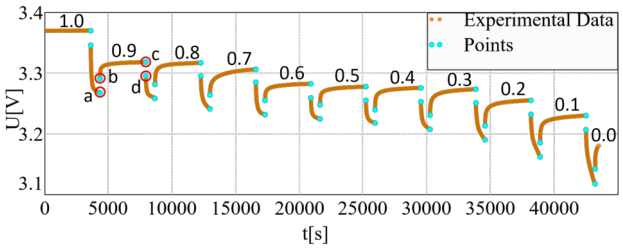

Fig. 4. Key points at each SOC.

$$U_{output}(t) = U_{oc} + U_1(0)e^{-\frac{t}{\tau 1}} + U_2(0)e^{-\frac{t}{\tau 2}} + U_3(0)e^{-\frac{t}{\tau 3}}. \tag{2}$$

3.2 Lookup Table

After the acquisition of experimental data, the next step is to establish the lookup tables for each circuit component in the model. It is really important to find all key points correctly, which are represented by cyan points with one group marked by red circles in Fig. 4 for an example. In this research, slope is used to locate these key points, because segments of neighbouring key points a~b and c~d describe the instantaneous response of the battery, which can be used to calculate R_0.

Segment b~c describes the hysteresis response of the battery. With the double exponential regression method raised by Jacquelin (2009), an exponential function of (3) could be found to fit the curve in this period.

$$y = be^{px} + ce^{qx}. \tag{3}$$

Where:

$$y = U_{output}(t) - U_{oc};$$
$$b = U_1(0); \qquad p = -\frac{1}{\tau 1};$$
$$c = U_2(0); \qquad q = -\frac{1}{\tau 2}.$$

It has been proved by Jackey et al. (2013), that simulation error depends on the initial fitting result. As shown in Fig. 5, the voltage difference ΔU at the initial recovery moment may have a significant influence on the whole simulation result because of the cumulative effect. Therefore, the third RC branch is added to compensate such an error, as presented in (4).

$$\Delta U = de^{0r} = d. \tag{4}$$

Where:

$$d = U_3(0); \qquad r = -\frac{1}{\tau 3}.$$

When the voltage begins to recover, it means SOC is a stable value, because there is no flowing current from the battery. Then all known parameters and experimental values could be put into (5) to get a large amount of values of r at each sampling instant. Then the mean value has to be calculated by (6), where N is the total number of values.

$$y = be^{px} + ce^{qx} + de^{rx}. \tag{5}$$

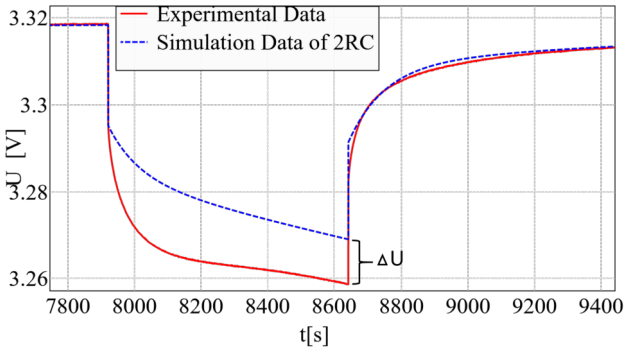

Fig. 5. Simulation result of 2 RC branches.

$$r = \frac{1}{N}\sum_{n=1}^{N}\frac{\ln(\frac{\Delta y}{d})}{x}. \tag{6}$$

In combination with (2), the time constants τ for these three RC branches can be obtained. As a result of the long "cool down" time before the next discharging, the polarization voltage inside can be neglected. In other words, the output voltage of discharging pulses can be viewed as the zero state response of RC branches, represented by (7) (8) (9).

$$U_1(t) = IR_1(1 - e^{-\frac{t}{\tau 1}}). \tag{7}$$

$$U_2(t) = IR_2(1 - e^{-\frac{t}{\tau 2}}). \tag{8}$$

$$U_3(t) = IR_3(1 - e^{-\frac{t}{\tau 3}}). \tag{9}$$

At the recovery instant from point a to b, the polarization voltage does not change basically, so the following equations could be further obtained (see Yan et al. (2018)).

$$U_1(0) = IR_1(1 - e^{-\frac{t_k}{\tau 1}}). \tag{10}$$

$$U_2(0) = IR_2(1 - e^{-\frac{t_k}{\tau 2}}). \tag{11}$$

$$U_3(0) = IR_3(1 - e^{-\frac{t_k}{\tau 3}}). \tag{12}$$

With t_k representing the discharging interval in (10) (11) (12), R_1~R_3 can be determined. Furthermore, with the help of τ, C_1~C_3 are obtained. Finally the lookup tables for all elements from $SOC = 0.9$ to $SOC = 0.1$ are generated, take the lookup table of C_1 in Table 2 for an example. The process of parameter estimation is explained in detail in Algorithm 1.

4. MODELING AND VALIDATION

In order to validate the parameters, the Third-order Thevenin model is developed in SIMBA$^{\#}$ (see ifak (2018)), with the one-dimensional lookup tables plugged into each module (see Fig. 6).

After the simulation of discharging, a comparison between experimental and simulation data is shown in Fig. 7. In this figure, the red solid line represents the measurement

Algorithm 1: *Parameter Estimation*

Input: U_{output}, t_{acc}
Output: R_0, U_{oc}, lookup tables for RC branches
while $t < t_{end}$ **do**
  find: key points;
  if $t_a < t < t_b$ **then**
    $R_{01} \leftarrow \Delta U_{ab}/I$;
  else
    if $t_b < t < t_c$ **then**
      Exponential Regression: b, c, d, p, q, r;
      $U_1(0), U_2(0), U_3(0) \leftarrow b, c, d$;
      $C1, R1 \leftarrow p$;
      $C2, R2 \leftarrow q$;
      $C3, R3 \leftarrow r$;
    else
      if $t_c < t < t_d$ **then**
        $R_{02} \leftarrow \Delta U_{cd}/I$;
      end
    end
  end
  $R_0 \leftarrow (R_{01} + R_{02})/2$;
  $U_{oc} \leftarrow U_c$;
end

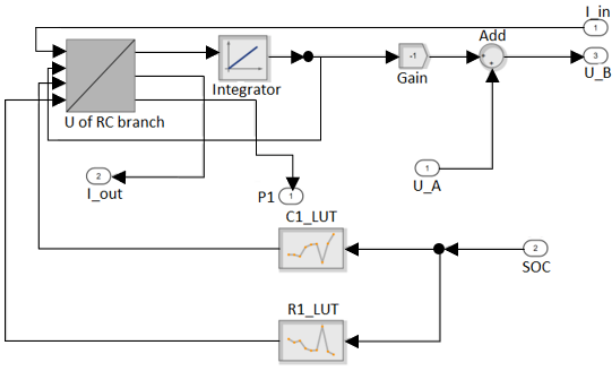

Fig. 6. Details of $RC1$ branch.

data of output voltage, the simulation result is displayed by the green dashed line.

Overall, the model fits the experimental data very well, except the discharging intervals when the SOC is not certain and all parameters are changing over time, which can not be determined simply by lookup tables. Furthermore, the relative residual error for each data point is calculated and shown in Fig. 8.

As mentioned before, there is little error at stable SOC levels, while larger error exists in discharging intervals.

Table 2. Lookup table for C_1

SOC	C [F]
0.1	47807.4
0.2	47530.4
0.3	44183.6
0.4	62687.7
0.5	67919.9
0.6	69244.5
0.7	32429.6
0.8	69875.2
0.9	88649.5

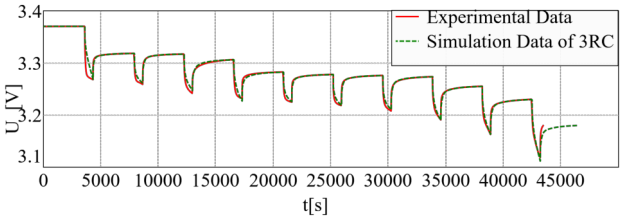

Fig. 7. Comparison between experimental and simulation data.

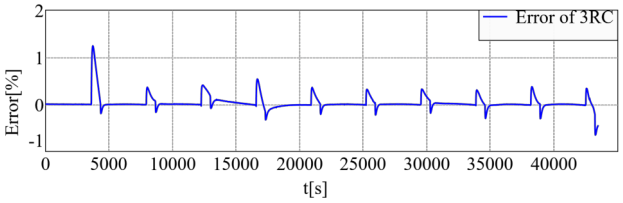

Fig. 8. Residual error of the circuit model.

However, the error in the first discharging interval (i.e. the transition period from $SOC = 1.0$ to $SOC = 0.9$) is caused by lack of lookup table values at $SOC = 1.0$, because the initial state of the battery is fully "cooled down", there is no polarization voltage inside RC branches. After calculation, the mean residual error for all points is 1.98 mV, the relative error is 0.061%. Removed of the first period before $SOC = 0.9$ and after $SOC = 0.1$, the mean residual error is updated to 1.60 mV, and the relative error becomes 0.049%. Therefore, this equivalent circuit model is validated to meet general demands on a system level to cooperate with other models powered by batteries.

5. SOC ESTIMATION FOR REAL BEB RUNNING

In this paper, a model for a single lithium-battery cell of 3.3 V is built up to estimate the SOC of an on-board battery pack for a real electric bus running. In order to simulate the energy consumption of a real BEB, a general control model of an electric bus with power train, applied by Czogalla and Jumar (2019), is adopted.

As shown in Fig. 9, the trip driving cycles, which describe the velocity at each moment, are firstly input to the whole control model. Then the model has to compare the real velocity with the pre-defined value in the cycles, to tell the driver to accelerate or decelerate, which is simulated by a PI-controller. If the bus is accelerated, the power supplying is calculated by the motor torque T_mot multiplies rotation speed ω. Considering the regenerative power to the battery system and the auxiliary power (e.g. heating, air condition, and lightening system), the required power from the battery model can be finally calculated, which is described in the form of current pulses. In addition, if the braking pedal is stepped on, a braking force F_b will work on the traction force F_tr, together with the aerodynamic force F_aero, rolling resistance F_rr and grade force F_grade, the inertia force F_i will be calculated via (13). Then F_i will accelerate the vehicle to update the velocity for the next moment. Table 3 lists the parameters of Solaris® electric bus for this simulation (see Bruge et al. (2016)).

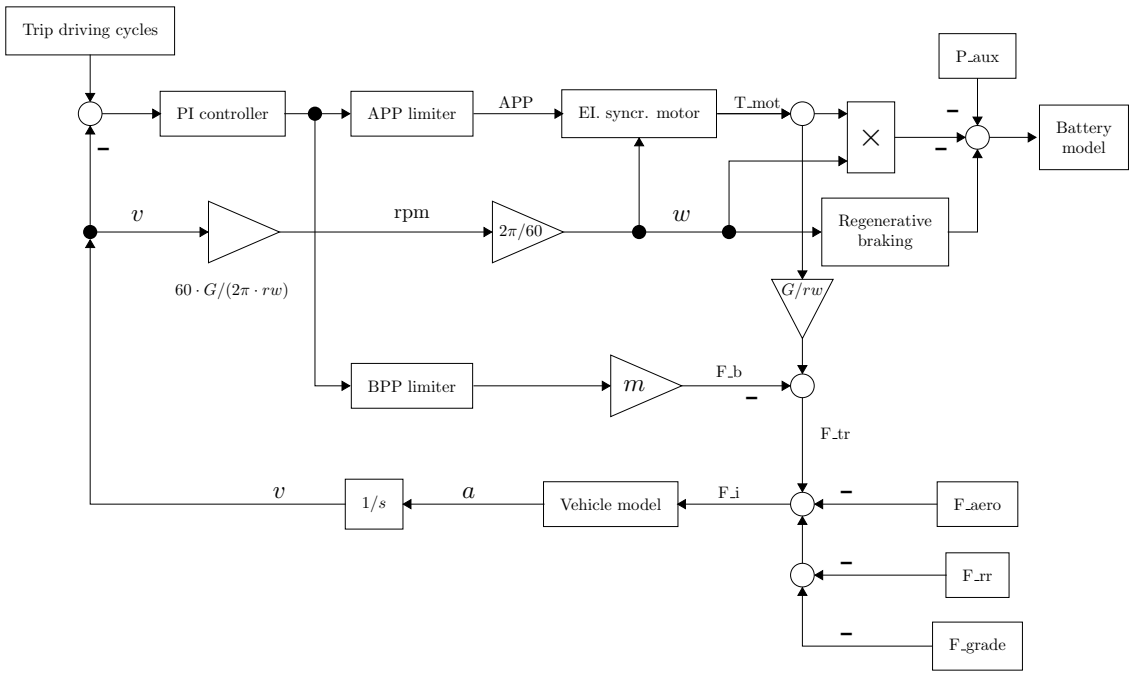

Fig. 9. General control model of an electric vehicle.

$$\begin{aligned} F\_tr &= F\_aero + F\_rr + F\_grade + F\_i \\ &= C_{rr} \cdot m \cdot g + C_d \cdot A_f \cdot \frac{\rho}{2} \cdot v^2 \\ &+ m \cdot g \cdot \sin(\phi) + m \cdot a. \end{aligned} \tag{13}$$

Where:

C_{rr} is rolling resistance coefficient, m is vehicle mass, g is gravitational acceleration, C_d is drag coefficient, ϕ is road angle in radians, ρ is air density, A_f is vehicle frontal area, v represents vehicle speed, and a is vehicle acceleration.

Table 3. Technical data of BEB for simulation

Model	Solaris® Urbino 12 Electric
Battery capacity	240 kWh
U_{oc}	600 V
Accessory load	5 kW
Max. power	250 kW
Max. torque	973 Nm
Frontal area	8.66 m^2
Final gear drive ratio	22.6
Mass/Load	13,790 kg/5, 100 kg

After combination of battery model and BEB driving model, one realistic bus route is generated as the input to the system. The simulation result is displayed in Fig. 10.

Considering real driving plans, 18 duty cycles are simulated for the full day round trips between Terminal 1 and Terminal 2. As shown in Fig. 10, Terminal 1 is the starting point, when the bus is driven towards Terminal 2 over a distance of 11 km, the SOC will drop down. Then the return trip still needs to consume the energy until it reaches Terminal 1 again, where a charging station is implemented for an opportunity charging (OPP), so the SOC will recover to a certain level. For fast charging, the selected power is 120 kW with a current of 200 A, the charging time is 5 min. Finally, after full day operation over 15 h, the bus has to be pulled into the depot for a slow charging. The result shows that the lowest SOC during service is about 72.69%. Thus at the depot, the electric bus needs to be charged for $(1 - 0.7269) \times 400\text{Ah} \div 50\text{A} \approx 2.2\text{h}$, with a charging power of 30 kW and current of 50 A.

6. CONCLUSION

In this research, a battery model in connection with a general electric vehicle driving model is successfully developed and validated, which cuts down the complexity largely while simultaneously reaches a small error. On a system level, it can estimate the SOC of the on-board battery for a full day operation. For real case simulation, parameters from an existing BEB are selected and the round trips between two terminals are generated based on the practical routes and schedules. Since the lowest SOC is 72.69%, it proves that the capacity of the battery with 240 kWh is sufficient for these duty cycles with only an opportunity charging for 5 min at Terminal 1. Even for slow charging, it only needs 2.2 h, which is possible for more BEBs charged at the depot overnight. This system provides a reliable estimation on the SOC for a specific bus route with inputs of several technical data, such as specification of BEB and charging conditions. Therefore, it can be adjusted to meet the requirements of operators to convert the bus fleet to a 100% electric bus fleet step by step.

In conclusion, this work validates the accuracy of this battery model on a system level and good portability, especially in cooperation with the electric bus driving model. A future work could be to measure the recovery voltage at $SOC = 100\%$ and $SOC = 0\%$ to add more values to lookup tables, which will consequently improve the accuracy.

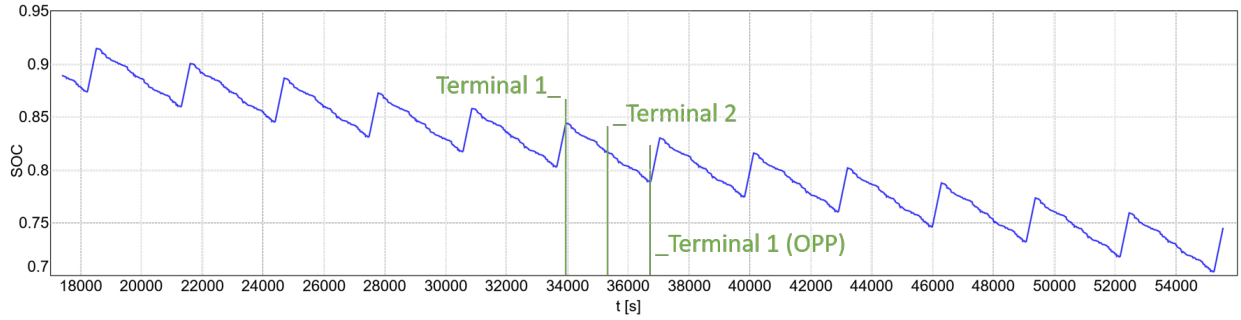

Fig. 10. SOC for 18 duty cycles.

REFERENCES

Aber, J. (2016). Electric bus analysis for new york city transit. *Columbia University, Nowy Jork*.

Adheesh, S., Vasisht, S.M., and Ramasesha, S.K. (2016). Air-pollution and economics: diesel bus versus electric bus. *Current Science*, 110(5), 858–862.

Asaithambi, G., Treiber, M., and Kanagaraj, V. (2017). *Life Cycle Assessment of Conventional and Electric Vehicles*. doi:10.1007/978-3-030-03816-8_21.

BMU (2018). Electric mobility. URL `https://www.bmu.de/en/search/?id=1892&no_cache=1&L=1&q=electric+mobility`. Federal Ministry for the Environment, Nature Conservation and Nuclear Safety.

Bruge, P., Guida, U., and Goralczyk, M. (2016). Zeeus ebus report an overview of electric buses in europe. *ZeEUS project, Brussels*.

Ceraolo, M. (2000). New dynamical models of lead-acid batteries. *IEEE Transactions on Power Systems*, 15(4), 1184–1190. doi:10.1109/59.898088.

Czogalla, O. and Jumar, U. (2019). Design and control of electric bus vehicle model for estimation of energy consumption. In *5th IFAC Symposium on Telematics Applications Chengdu, China*. September 25-27.

Du, J., Li, F., Li, J., Wu, X., Song, Z., Zou, Y., and Ouyang, M. (2019). Evaluating the technological evolution of battery electric buses: China as a case. *Energy*, 176, 309 – 319. doi: https://doi.org/10.1016/j.energy.2019.03.084. URL `http://www.sciencedirect.com/science/article/pii/S0360544219304888`.

European Commission (2011). Roadmap for moving to a competitive low-carbon economy in 2050.

Gao, L., Liu, S., and Dougal, R.A. (2002). Dynamic lithium-ion battery model for system simulation. *IEEE Transactions on Components and Packaging Technologies*, 25(3), 495–505. doi:10.1109/TCAPT.2002.803653.

Göhlich, D., Kunith, A., and Ly, T. (2014). *Urban Transport XX*, volume 138, chapter Technology assessment of an electric urban bus system for Berlin, 137–150. WIT Press. doi:10.2495/UT140121. Online.

Grijalva, E.R. and López Martínez, J.M. (2019). Analysis of the reduction of CO2 emissions in urban environments by replacing conventional city buses by electric bus fleets: Spain case study. *Energies*, 12(3), 525.

Huria, T., Ceraolo, M., Gazzarri, J., and Jackey, R. (2012). High fidelity electrical model with thermal dependence for characterization and simulation of high power lithium battery cells. In *2012 IEEE International Electric Vehicle Conference*, 1–8. doi: 10.1109/IEVC.2012.6183271.

ifak (2018). *Simba# 3.0*. ifak e.V. Magdeburg. URL `https://simba.ifak.eu`.

Jackey, R., Saginaw, M., Sanghvi, P., Gazzarri, J., Huria, T., and Ceraolo, M. (2013). Battery model parameter estimation using a layered technique: An example using a lithium iron phosphate cell. In *SAE Technical Paper*. SAE International. doi:10.4271/2013-01-1547. URL `https://doi.org/10.4271/2013-01-1547`.

Jacquelin, J. (2009). Régressions et équations intégrales. *Online]. https://www. researchgate. net/.../14674814-Regressions-et-equations-integrales. pdf*.

Klein, R., Chaturvedi, N.A., Christensen, J., Ahmed, J., Findeisen, R., and Kojic, A. (2013). Electrochemical model based observer design for a lithium-ion battery. *IEEE Transactions on Control Systems Technology*, 21(2), 289–301. doi:10.1109/TCST.2011.2178604.

Krawiec, S., Łazarz, B., Markusik, S., Karoń, G., Sierpiński, G., and Krawiec, K. (2016). Urban public transport with the use of electric buses - development tendencies. *Transport Problems*, Volume 11, 127–137. doi:10.20858/tp.2016.11.4.12.

Li, J.Q. (2016). Battery-electric transit bus developments and operations: A review. *International Journal of Sustainable Transportation*, 10(3), 157–169. doi:10.1080/15568318.2013.872737. URL `https://doi.org/10.1080/15568318.2013.872737`.

Smith, K.A., Rahn, C.D., and Wang, C.Y. (2007). Control oriented 1d electrochemical model of lithium ion battery. *Energy Conversion and Management*, 48(9), 2565 – 2578. doi: https://doi.org/10.1016/j.enconman.2007.03.015. URL `http://www.sciencedirect.com/science/article/pii/S0196890407000908`.

Tang, X., Wang, Y., Zou, C., Yao, K., Xia, Y., and Gao, F. (2019). A novel framework for lithium-ion battery modeling considering uncertainties of temperature and aging. *Energy conversion and management*, 180, 162–170.

UNFCCC (2015). The Paris Agreement. In *The Paris climate conference (COP21)*. URL `https://unfccc.int/process-and-meetings/the-paris-agreement/the-paris-agreement`.

Yan, H., Gan, X., Wu, H., and Liu, A. (2018). Modeling and simulation of lithium-batteries based on the second-order thevenin model. *Journal of Jiangsu University: Natural Science Edition*, 39(4), 403–408.